

Available at [www.sciencedirect.com](http://www.sciencedirect.com)journal homepage: [www.elsevier.com/locate/issn/15375110](http://www.elsevier.com/locate/issn/15375110)

## Research Paper

# Empirical description of granular flow inside a model silo with vertical walls

Irena Sielamowicz<sup>a,\*</sup>, Michał Czech<sup>b,1</sup>, Tomasz A. Kowalewski<sup>c,2</sup>

<sup>a</sup> Technical University, Civil Engineering Department, 15-196 Białystok, Matejki 8, Poland

<sup>b</sup> Białystok Technical University, Mechanical Department, 15-351 Białystok, Wiejska 45 C, Poland

<sup>c</sup> Institute of Fundamental Technological Research, Polish Academy of Sciences, 02-106 Warsaw, Pawińskiego 5B, Poland

## ARTICLE INFO

### Article history:

Received 16 July 2010

Received in revised form

9 December 2010

Accepted 7 January 2011

Published online 25 February 2011

DPIV (Digital Particle Image Velocimetry) is often used to record the flows in silo models and to recognise the flow in two-dimensional structures. Flow in a two-dimensional laboratory model with transparent walls was recorded using the DPIV technique. Recorded images were processed and the velocities of the flowing material were obtained. Statistical analysis of the readings taken from velocity profiles was also performed. To describe the flow the theoretical model of velocity presented in Choi, Kudrolli, and Bazant (2005) was modified. An empirical description of the flow rate was carried out. An analysis of the kinematic parameter  $b$  was carried out and compared to the solutions given by Medina, Córdova, Luna, and Treviño (1998) and Choi et al. (2005). Comparisons between the experimental measurements and the empirical descriptions are presented. Comparing the Gaussian based kinematic model of Choi et al. (2005) and a modified empirical kinematic model, a better description of velocity was obtained by using the latter. In further comparisons using the two aforementioned models and a parabolic description the best description of velocity was given by the parabolic function. Flow rate was analysed using the three types of functions. Both the Gaussian and modified empirical kinematic model gave almost the same values for calculated levels  $h = 5, 10$  cm. Using the parabolic description the value of flow rates differed slightly. The flow channel boundary was analysed using parabolic and hyperbolic descriptions. Both descriptions were good because the correlation coefficients, had values ranging from 0.928 to 0.997.

© 2011 IAGrE. Published by Elsevier Ltd. All rights reserved.

## 1. Introduction

Typical granular flows occurring in silos and hoppers are usually dense. As was stated in Choi et al. (2005) a fundamental

statistical theory is not available to describe their properties and there is a lack of quantitative data to help develop models of dense granular flows. In this paper, the nature of dense granular flow is investigated and the results analysed using

\* Corresponding author. Tel./fax: +48 85 6755 997.

E-mail addresses: [irena.sielamowicz@gmail.com](mailto:irena.sielamowicz@gmail.com) (I. Sielamowicz), [mceh@pb.bialystok.pl](mailto:mceh@pb.bialystok.pl) (M. Czech), [tkowale@ippt.gov.pl](mailto:tkowale@ippt.gov.pl) (T.A. Kowalewski).

<sup>1</sup> Tel.: +48 85 7469307; fax: +48 85 7469559.

<sup>2</sup> Tel.: +48 22 8285373; fax: +48 22 8269815.

1537-5110/\$ – see front matter © 2011 IAGrE. Published by Elsevier Ltd. All rights reserved.

doi:10.1016/j.biosystemseng.2011.01.004

Nomenclature	
PIV	particle image velocimetry
DPIV	digital particle image velocimetry
OF-DPIV	optical flow digital particle image velocimetry
K	statistical criteria
$\alpha$	significance level
$\bar{V}_y$	average vertical velocity
S	standard deviation
n	number of readings
x	distance from the axis of symmetry
t	time
h	given level, height
$\varphi_w$	wall friction
$\varphi_e$	angle of internal friction
$\rho_b$	granular material density deposited through a pipe with zero free-fall
r	coefficient of correlation
f(z)	Lagrange polynomial
$V_y$	vertical velocity measured in experiments
$V_{av}$	average velocity
A, B, C	parameters
P	the probability
t	variable of Student t test
$A_i (A_0, A_1, A_2), B_i (B_0, B_1, B_2)$	parameters in Eq. (3)
$v(x, z)$	velocity in a point
b	kinematic parameter
$x_{max}$	values of abscissa
(20, 50)	interval for variable values of height
$t_\alpha$	abscissa, the left limit of the area $\alpha$
$t_{n-1, 1-\frac{\alpha}{2}}$	quantile of Student t distribution
$t_{n-1, 1-\frac{\alpha}{2}\frac{S}{\sqrt{n-1}}}$	half of the confidence interval
$V_{av} - t_{n-1, 1-\frac{\alpha}{2}\frac{S}{\sqrt{n-1}}}$	lower limit of the confidence interval
$V_{av} + t_{n-1, 1-\frac{\alpha}{2}\frac{S}{\sqrt{n-1}}}$	upper limit of the confidence interval
$V_y$	is the i-th reading taken from the experiments for all time instants
$V_{av}$	the average value of experimental readings
z	variable location of level
i = 0, 1, 2	indices
Q	flow rate
$\hat{x}$	distance from the axis of symmetry to the boundary of the flow for various time instants
$\langle \bar{v} \rangle$	the dimensionless average vertical velocity
$\langle \bar{v}_0 \rangle$	initial vertical velocity
B	dimensionless fitting parameter
$\hat{x} = x/W, \hat{y} = y/W$	W, width of the model in Medina et al. (1998)
H	width of the model in Medina et al. (1998)
$V_0$	initial velocity
$a_1, b_1, a_2, b_2$	constant values in Formulae 13, 14

a modified empirical descriptions of the velocities of the granular material and the solutions given in Medina et al. (1998) and Choi et al. (2005).

Both dense and loose flows have been investigated in physical models or *in situ*. However, there is still a lack of quantitative data to investigate models of dense granular flows. In this paper, the nature of the flow is investigated to devise an empirical description of velocities of granular material. Several experimental and theoretical efforts have been directed mainly towards understanding the velocity within the flow region (Brown & Richards, 1970; Haüssler & Eibl, 1984; Hirshfeld, Radzyner, & Rapaport, 1997; Hong & McLennan, 1992; Kafui & Thornton, 1997; Khelil & Roth, 1994; Nedderman, 1992; Sakaguchi, Ozaki, & Igarashi, 1993; Srinivasa, Nott, & Kesava, 1997; Tüzün, Houlsby, Nedderman, & Savage, 1982; Wang, Gardner, & Schaeffer, 1992). Few theoretical studies have analysed the whole velocity field in steady-state flow, (Wang et al., 1992) or in time-dependent flow (Haüssler & Eibl, 1984; Hong & McLennan, 1992).

Several aspects of granular flows have been also studied over the years. Two of the most important are the flow rate and the velocity field. Beverloo, Leniger, and de Velde (1961) formulated a relationship between orifice size and mass flow rate. Velocity fields in silos have also been studied by several researchers using different measurement techniques. To investigate granular flows in laboratory models techniques have included X-ray imaging, ultrasonic measurements or the use of transparent walls. Other non-invasive measurement techniques have been applied to register granular flows, density and velocity fields in flowing zones. Techniques used with spy-holes have included radio transmitters, positron

emission, magnetic resonance imaging, radioactive tracers, and ultrasonic speckle velocimetry. More details on different techniques used in the investigations of granular flow in scale models can be found in references given by Ooi, Chen, and Rotter (1998) and by Lueptow, Akonur, and Shinbrot (2000), where the application of particle image velocimetry (PIV) was recommended to study quasi two-dimensional flows in transparent containers. Some of the first successful attempts to apply the PIV technique to granular matter were described by Medina et al. (1998) and by Waters and Drescher (2000). More recently Böhrens, Ostendorf, Antes, and Schwedes (2004), Ostendorf and Schwedes (2005), Sielamowicz, Błoński, and Kowalewski (2005, 2006), Choi et al. (2005), Niedostatkiwicz and Tejchman (2005), Steingart and Evans (2005) reported the use the PIV techniques in their experiments to obtain information on local velocities of particles at several elevations in the densely packed materials. Application of the digital particle image velocimetry (DPIV) technique to granular flows in two-dimensional hoppers appears to be very promising. Despite its limitations (only flows close to a transparent wall are observed), the DPIV technique offers the possibility of obtaining full-field transient velocity fields, and by applying standard mechanical relationships, offering the possibility of evaluating the distribution of shear stresses in the material.

The basic assumptions introduced by Jenike (1961, 1964) for the radial stress and velocity fields in flowing granular materials have been used by many engineers in theoretical and experimental investigations. In theoretical models of granular flow the assumption of incompressibility throughout the hopper is an essential element in the predictions of velocities and flow boundaries (Drescher, 1991). Mathematical models

introduced into the analyses assume a rigid perfect plastic model or purely kinematic material model, as proposed by Litwinişzyn (1963), further developed by Mullins (1972, 1979) and applied by Nedderman and Tüzün (1979), Waters and Drescher (2000), or in a revised form by Drescher and Ferjani (2004). Nedderman (1995) presented a theoretical model for the process of unsteady discharge, based on the incompressible radial velocity field resulting from the kinematic theory. The kinematic model predicted velocity fields with only one free parameter  $b$ . This parameter was observed to be proportional to grain diameter in all experimental tests. Medina et al. (1998) analysed the flow in detail by the PIV technique and studied that the kinematic parameter varies within a silo. Choi et al. (2005) presented a wide review on models for the mean velocity profiles. The vector field obtained from PIV has been used to calculate lines tangential to the instantaneous velocity, called streamlines in fluid mechanics. In granular material flows one usually visualises a track of individual particles, not necessarily coinciding with the streamline. Such tracks were obtained by Choi et al. (2005), who used a high-speed imaging technique to trace the position of single particles in granular material.

Therefore, an experimental evaluation of the velocity field appears necessary to obtain quantitative information of the gravity-induced flow. Here, velocity fields and velocity profiles in a two-dimensional physical model presented and the data are used to describe the dependence of vertical velocity on some factors. A series of experimental results analysing funnel flow is used to relate the non-steady granular flow and its spatial and temporal fluctuations. The assumption of Drescher (1991) that the density of the flowing material does not change is investigated.

## 2. Experimental method for the DPIV measurements

Flow in a plane flat-bottomed model silo with central filling and central discharge was investigated. The images of the flowing material were recorded by a high-resolution camera and evaluated using the DPIV technique. The adopted DPIV technique was based on the optical flow algorithm (OF-DPIV), which has been found to be most reliable for granular flow images. Quenot, Pakleza, and Kowalewski (1998) presented a detailed description of the OF-DPIV, including its development and application. A velocity vector is obtained for every pixel of the image. Calibration, carried out for synthetic sequences of images, showed that the accuracy of measured displacement was about 0.5 pixel frame<sup>-1</sup> for tested two-image sequences and 0.2 pixel frame<sup>-1</sup> for four-image sequences. The experimental setup used for the flow analysis consisted of a transparent acrylic plastic box, a set of illumination lamps, and a high-speed CCD camera (PCO1200HS) with an objective 50 mm lens, presented in Fig. 1 (after Sielamowicz et al., 2005) produced by PCO AG, Kelheim, Germany, [<http://www.pco.de/high-speed-cameras/pco1200-hs/>]. The transparent flat-bottom silo model had a height of 800 mm, a depth of 100 mm, and a width of 260 mm and was constructed in transparent acrylic plastic. The model was placed on a stand and granular material was supplied through

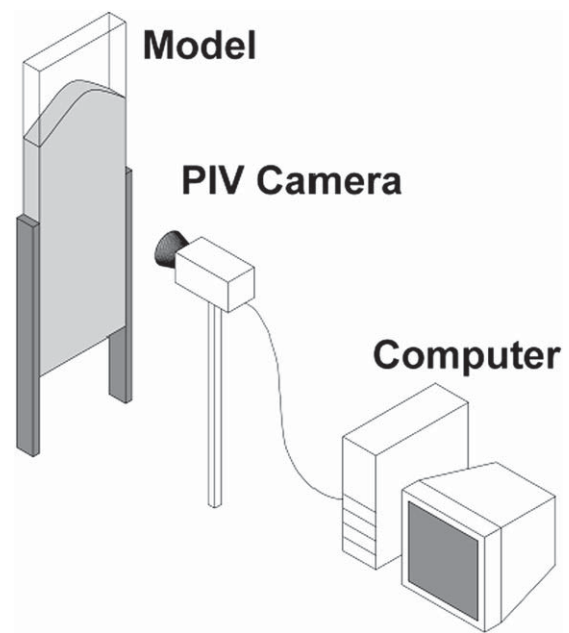


Fig. 1 – Schematic diagram of the experimental equipment, after Sielamowicz et al. (2005).

a box suspended above the model. The bottom of the supplying box contained a sieve and the box was filled with granular material to 2/3 of its height. The model was filled centrally along its axis of symmetry. The discharge outlet was located centrally at the bottom of the silo. The width of the outlet was 10 mm. In order to evaluate transient velocity fields, long sequences of 100–400 images were taken at variable time intervals, covering the whole of the discharge time. The DPIV technique used here produced velocity fields for the full interrogation area. The velocity profiles obtained inside the quasi two-dimensional silo were smooth and free of shock-like discontinuities.

Amaranth seed was used in the experiments. The material showed some effects of static electricity when flowing and sliding over the transparent acrylic plastic. The granular material was introduced through the sieve in a form of a uniform stream into the silo model to obtain uniform and repeatable packing of the material with no particle segregation. The construction of the model allowed different inclinations of the silo bottom to the vertical. However, the present description is limited to the flat-bottomed silo only.

The evolution of the flow region and the traces of flowing particles were evaluated from recorded images. Pairs of digital short exposure images were taken to describe how the velocity field varies in the flowing material. This data was used in empirical description of the flow. The mechanical data of the amaranth seed were obtained in the laboratory. The properties of the amaranth seed used in the experiments were; wall friction against transparent acrylic plastic  $\phi_w = 25^\circ$ , angle of internal friction  $\phi_e = 28^\circ$ , granular material density deposited through a pipe with zero free-fall  $\rho_b = 832 \text{ kg m}^{-3}$  at 1 kPa and  $\rho_b = 833 \text{ kg m}^{-3}$  at 8 kPa, Young's modulus 12.96 MPa.

### 3. Analysis of experimental results

In Fig. 2 velocity profiles are shown, they are symmetrical in their form. A high velocity flow region was located in the vicinity of the outlet. In data processing using the DPIV technique vector fields were obtained and streamlines calculated from the velocity fields measured in the model (Sielamowicz et al., 2005). Although the flow was symmetrical some disturbances in the flow of single particles, especially close to

the outlet, were observed. The grains were less homogeneous and contained some natural pollutants. The shape and size of the grains, the nature of the seed surface, and the moisture content of the granular material influences the flowing properties of grains.

Another step in processing the DPIV results is obtaining velocity profiles. The velocity profiles shown in Fig. 2a–f were obtained for use in the analysis to describe variations in vertical velocity. The results taken from vertical velocity profiles from Fig. 2a–f are also presented in Tables A1–A6 in

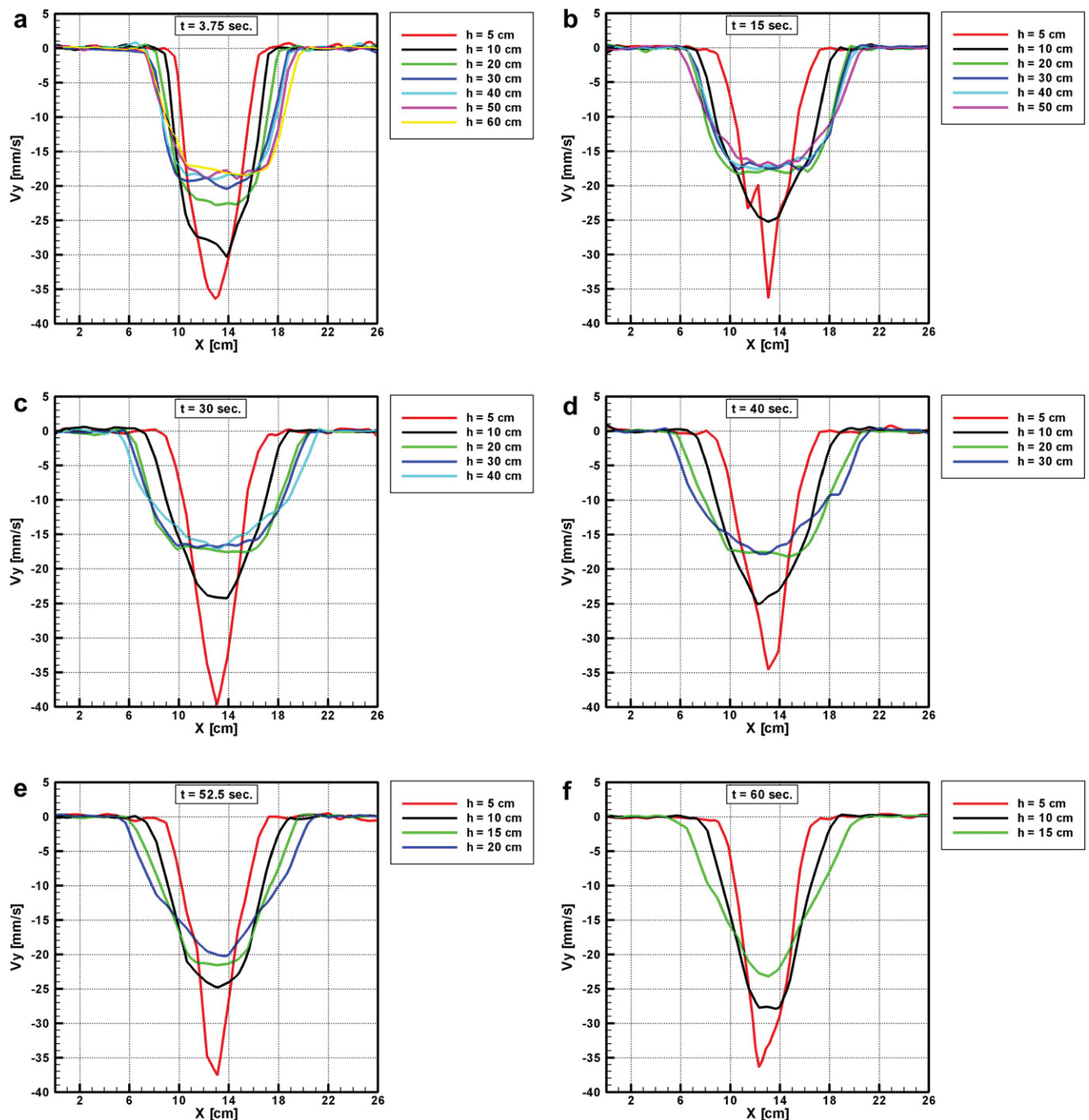


Fig. 2 – Velocity profiles of flowing amaranth seeds shown at given times and for different levels, (Sielamowicz et al., 2005). The coloured lines denote the velocities at height  $h$  in the model measured from the outlet.

the Electronic Appendix. The results showed that velocities had different values at levels  $h = 5$  and  $10$  cm above the outlet during the whole period the material flowed. However, vertical velocity profiles at the levels  $> h = 20$  cm were almost uniform.

#### 4. Description of the flow

The whole of the velocity field had very interesting and complex properties. Here, the intensity of the velocity fluctuations is characterised at several selected heights from the bottom of the hopper. The funnel flow was divided into three zones as can be seen in Fig. 3. At the top of the hopper was the *inflow zone* which covers the width of the model but narrowed to the central zone, the *steady state zone* with vertical boundaries. The velocity vectors moved from being directly radial in the *inflow zone* into being vertical in the *steady state zone* and again radial in the *outflow zone*.

The upper surface of the packed material, made flat after filling, altered its profile while the material flowed. It became nearly conical in the final stages of the flow. In stagnant zones, formed on the sides of the funnel flow, the measured velocities were zero. In the plug-flow region in the *outflow zone* the velocity vectors in the initial phase of flow were vertical, indicating the absence of measurable lateral displacement. In the upper part of the flow the velocity vectors indicated converging lateral flows towards the flowing zone. The high velocity flow region was located in the vicinity of the outlet. In the final phase of the flow, the high velocity region at the outlet spread upwards into the plug-flow zone. The flow was almost symmetrical but some disturbances of single particles, especially near the outlet, were observed.

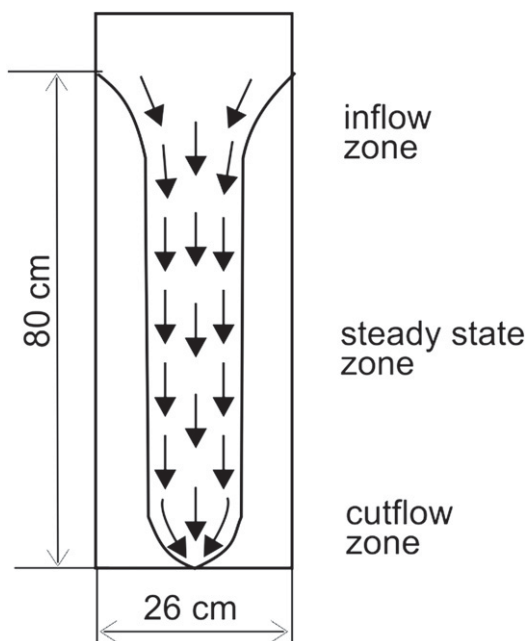


Fig. 3 – Flow zones in the model.

**Table 1 – Parameters A, B from Eq. (2) determined by the Least Square Method using the values  $V_{av}$  from Tables A, B, C presented in Appendix.**

Parameter value	A	B	R-correlation coefficient
$h = 5$ cm	40.13	-0.242	-0.9942
$h = 10$ cm	30.86	-0.1008	-0.9763
$h = 20$ cm and higher levels	22.82	-0.0508	-0.9628

#### 5. Empirical analysis of vertical velocity ( $V_y$ )

##### 5.1. Empirical description of velocities

An empirical description of velocities in the model was carried out. An initial analysis of velocity was made using an equation presented in Choi et al. (2005), but this was followed by two modifications of that equation.

##### 5.1.1. Analysis of velocity by the kinematic model

A Gaussian solution of for velocity distribution in a silo was presented in Choi et al. (2005) in the form:

$$v(x, z) = \frac{Q}{\sqrt{4\pi bz}} e^{-x^2/4bz} \quad (1)$$

where  $v(x, z)$  denotes velocity in a point,  $Q$  – flow rate,  $z$  – height of the considered point. The constant of proportionality  $b$  in Eq. (1) was called “diffusion length” by Choi et al. (2005) but is commonly called the kinematic parameter. The solution was developed for a semi-infinite quasi two-dimensional system ( $-\infty < x < +\infty$ ) with a point-like orifice at  $z = 0$  which acts as a source of velocity. In Eq. (1) the variable  $z$  should be greater than zero. In our case  $z$  ranged from 5 to 60 cm. Here a point-like orifice was not considered. There was no need to introduce the new location of the orifice because the location of the outlet was fixed and this level was treated as the origin of the coordinate system. The real position of the orifice makes no significant difference in the analysed measurements. The distance between the real outlet, and the point-like assumed orifice, denoted as  $z_0$ , was small because the tangents to the velocity profiles converged very close to the outlet.

The kinematic model predicts velocity fields with only one free parameter,  $b$ . Although the free parameter was determined to be proportional to grain diameter, the constant of proportionality has been found not to agree (Mullins, 1974; Samadani, Pradhan, & Kudrolli, 1999; Tüzün & Nedderman, 1979). Medina et al. (1998) investigated the variation of the kinematic parameter inside a silo recording the flow in detail using the PIV. The kinematic model was also tested experimentally and the parameter  $b$  was measured by a number of

**Table 2 – Values of parameters  $A_i$  and  $B_i$  determined from Eq (6) and values given in Table 1.**

Parameters	$I = 0$	$I = 1$	$I = 2$
$A_i$	52.9	-2.904	0.07
$-B_i$	0.4607	-0.05148	0.001549

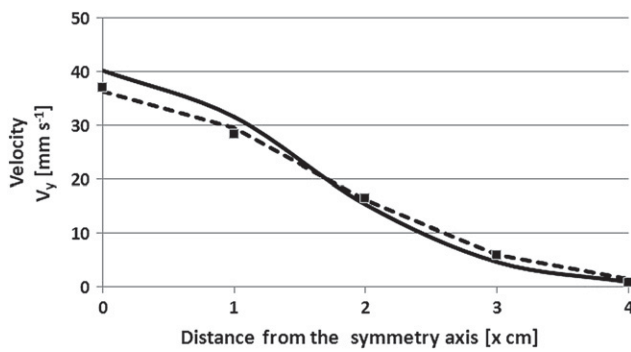


**Fig. 4 – Comparison of velocity values: experimental results – squares; with – empirical kinetic model (Eqs. (2), (3), Table 2) – the solid line and modified kinetic empirical model (Eq. (4) and Table 3) the dashed line, for level  $h = 5$  cm.**

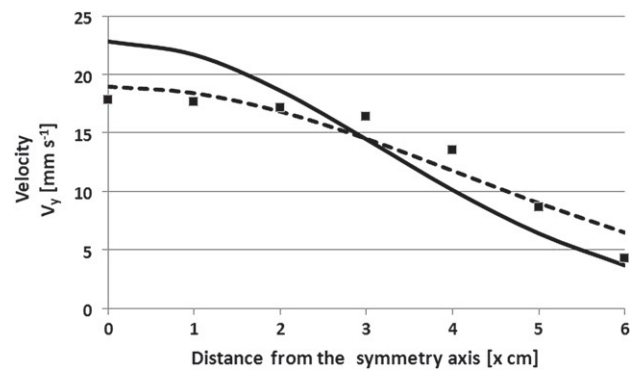


**Fig. 6 – Comparison of velocity values: experimental results – squares with kinetic empirical model (Eqs. (2), (3), Table 2) – the solid curve and modified kinetic empirical model (Eq. (4) and Table 3) – the dashed curve, for level  $h = 20$  cm.**

other researchers. For example, Tüzün and Nedderman (1979) determined that  $b \approx 2.24 d$  for various particle sizes, Mullins (1974)  $b \approx 2 d$  for iron ore particles, and Medina et al. (1998) found that diffusion length varies from  $b \approx 1.5 d$  to  $4 d$ . Samadani et al. (1999) proposed  $b \approx 3.5d$  for monodisperse glass beads. Choi et al. (2005) stated that a single fitting parameter  $b$  was sufficient to reproduce the entire flow field and this should be viewed as a major success of the kinematic model.

**5.1.2. Analysis of velocity by an empirical kinematic model**  
Another approach is to use an empirical description of velocity distribution. Sielamowicz, Czech, and Kowalewski (2010) presented the vertical velocity using  $V_y = e^{A+Bx+Cx^2} = De^{Bx+Cx^2}$ , where an eccentric flow was described. The granular material used in their experiment was flax seed. In the case examined here, with symmetric flow, and the expression  $Bx$  can be removed. Therefore, analysing velocities in the flowing material the following description for vertical velocity, defined as the empirical kinematic model, is proposed:

$$V_y(x) = Ae^{Bx^2} \tag{2}$$

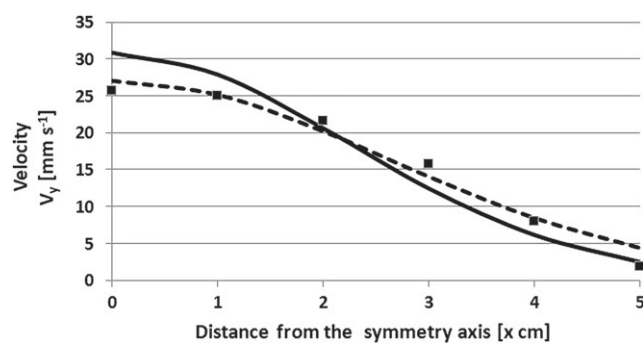


**Fig. 5 – Comparison of velocity values: experimental results – squares; with empirical kinetic model (Eqs. (2), (3), Table 2) – the solid curve and modified kinetic empirical model (Eq. (4) and Table 3) – the dashed curve, for level  $h = 10$  cm.**

where  $A$  and  $B$  are the parameters determined by the least squares method using the data from Tables A15, A16, A17 given in Electronic Appendix and summarised in Table A1. In Eq. (2) a distance  $x$  from the axis of symmetry is introduced in cm and velocity  $V_y(x)$  in mm s $^{-1}$ . Parameter  $A$  has the units of velocity mm s $^{-1}$  and parameter  $B$  has the unit of cm $^{-2}$ .

Taking the values from Table 1, parameters  $A$  and  $B$  were ascribed to the position of level  $z$ , and the velocities were calculated using an approximation of the second order polynomial of the Lagrangian type in the following form:

$$\begin{aligned} A &= A_0 + A_1z + A_2z^2 \\ B &= B_0 + B_1z + B_2z^2 \end{aligned} \tag{3}$$

In Eq. (3)  $z$  is defined in cm and  $A$  is obtained in the units mm s $^{-1}$ ,  $B$  in the units cm $^{-2}$ . The values of parameters  $A_i$  ( $A_0, A_1, A_2$ ) and  $B_i$  ( $B_0, B_1, B_2$ ) are listed in Table 2.

For values  $y \in (20, 50)$  parameters  $A$  and  $B$  were taken as for level  $h = 20$  cm.

The velocities described by the empirical model are presented in Figs. 4–6

**5.1.3. Analysis of velocity by a modified empirical kinematic model**

The empirical kinematic model presented by Eq. (2) was modified to the following function:

$$V_y = A(e^{-Bx^2} + e^{-Cx^2}) \tag{4}$$

Using the non-linear regression (Gauss-Newton method) the parameters  $A, B$  and  $C$  in Eq. (4) were determined and their values listed in Table 3. Velocity  $V_y$  was again calculated in

<b>Table 3 – Parameters <math>A, B, C</math> from Eq. (4) determined by the LSM using the values <math>V_{av}</math> from Tables A, B, C presented in Electronic Appendix.</b>			
Level $h$ (cm)	$A$	$B$	$C$
5	18.083	0.203	0.203
10	13.523	0.073	0.073
20 and higher levels	9.480	0.0304	0.0304

mm s<sup>-1</sup> and the distance from the axis of symmetry  $x$  in cm (Figs. 4–6).

Based on Eq. (4) and the values given in Table 3, the velocities were calculated and shown in Tables A7–A9 (given in Electronic Appendix). Examination of the model described by Eq. (2) showed that the given description in Eq. (4) practically reduces to Eq. (2). The above can be proved since the values obtained for parameters  $B$  and  $C$  in Eq. (4) and shown in Table 3 are all equal. It follows, therefore, that the model presented in Choi et al. (2005) and our description given in Eq. (2), provide sufficient accuracy for an empirical description of the flow. Some better results are obtained from the modified kinematic model (Eq. (4)), but they are derived from the method of determining parameters  $A$ ,  $B$  and  $C$  (i.e. non-linear regression) but not from the added term in Eq. (4). The parabola in Eq. (4) was created using non-linear regression, whereas Eq. (2) was transformed into the linear regression. In Figs. 4–6 the description of velocities by the kinematic model were compared to the modified kinematic model. The curves in these figures show that the description provided by the modified model was more accurate.

5.1.4. Evaluation of parameter  $b$  in the kinematic model

The structure of the velocity profiles obtained using the PIV technique did not change with the height. The kinematic model (Nedderman and Tüzün, 1979) showed a good fit. The parameter  $b$  was evaluated by comparing the corresponding coefficients in Eqs. (1) and (2) with the values from Table A1. The amaranth grains had a single particle size of 1 mm in diameter. For level  $h = 5$  cm above the outlet parameter  $b$  equals:

$$b = -\frac{1}{4Bh} = -\frac{1}{4(-0.242)5} = 0.2066 \text{ (cm)}$$

or  $b = 2.066 d$ , where  $d = 1$  mm is the diameter of the particle. For level  $h = 10$  cm, parameter  $b = 0.244$  (cm) or  $b = 2.44 d$ , for level  $h = 20$  cm, and higher levels, parameter  $b = 0.247$  (cm) or  $b = 2.47 d$ . Variations of the value of parameter  $b$  are shown in Fig. 7.

Medina et al. (1998) presented velocity profiles obtained using PIV and fitted the results using the correlations obtained using the kinematic model, hence the average value of the vertical velocity was in the form:

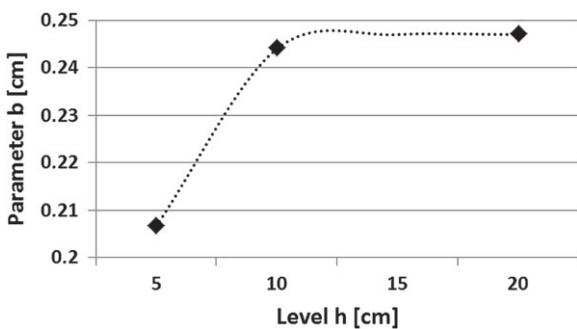


Fig. 7 – Variation of kinematic parameter  $b$  in the presented analysis.

$$\langle \hat{v} \rangle = \langle \hat{v}_0 \rangle \exp\left(-\frac{(\hat{x} - 1/2)^2}{4B\hat{y}}\right) \tag{5}$$

and

$$\langle \hat{u} \rangle = -B \frac{\partial \hat{v}}{\partial \hat{x}} = \frac{\langle \hat{v}_0 \rangle (\hat{x} - 1/2)}{2\hat{y}} \exp\left(-\frac{(\hat{x} - 1/2)^2}{4B\hat{y}}\right) \tag{6a}$$

where  $\langle \hat{v} \rangle$  is the dimensionless average vertical velocity,  $\langle \hat{v}_0 \rangle$  - initial vertical velocity,  $B$  is a dimensionless fitting parameter,  $\hat{x} = x/W$ ,  $\hat{y} = y/W$  and  $y$  is the vertical coordinate, measured from the bottom of the silo. Their experiments were performed in a vertical glass-walled silo model of 100 cm height,  $W = 30$  cm width and 3.8 mm deep, filled up to  $H = 82$  cm with a monodisperse granular material composed of spherical glass beads with mean diameter  $d = 3.15 \pm 0.04$  mm.

The average vertical velocities were determined using Eq. (5). If  $x = 0$  is substituted to Eq. (2) then the calculated initial value of vertical velocity  $\hat{V}_{y0}$  is obtained. It is assumed that this value is close to the average experimental value of vertical velocity.

Medina et al. (1998) considered the variation of kinematic parameter  $B$  at height  $h = 6$  cm and up to  $h = 20$  cm above the base of the model. The distribution of parameter  $B$  was given in a non-linear increasing function, (cf. Fig. 8). If this function is extrapolated above level  $h = 20$  cm in the model it would increase continuously. This would mean that kinematic parameter  $B$  would change continuously with the height in a non-linear form with no regions where it stabilises. In our analysis parameter  $b$  increases between the height  $h = 5$  cm and  $h = 10$  cm and then the parameter decreases (not shown). Fig. 9 presents the variation of parameter  $b$ , but using the data from Table A2 and Eq. (3) parameter  $b$  above the level  $h = 20$  cm decreases. This is the opposite situation to that described by Medina et al. (1998). The calculated values confirmed the fact that the kinematic parameter  $b$  was not a constant but it varies depending on the height in the model. The kinematic parameter  $b$  changed its value with the height in a non-linear form but up to level  $h = 10$  cm it increased significantly, by about 18%. Above this level the increase was only about 1%. The kinematic parameter stabilised above level  $h = 10$  cm, again the opposite situation to that described by Medina et al. (1998). Other authors, Tüzün et al. (1982), Kafui and Thornton (1997), Medina et al. (1998) also found that the kinematic parameter changed with the height. Based on Eqs.

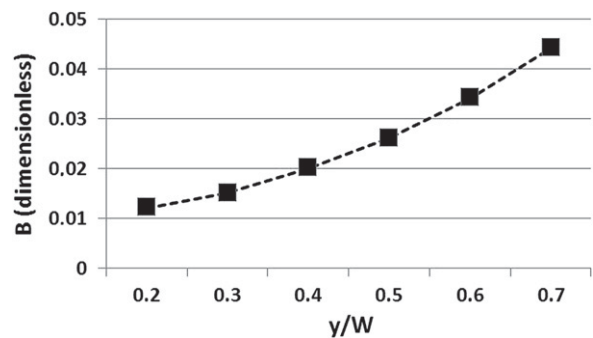
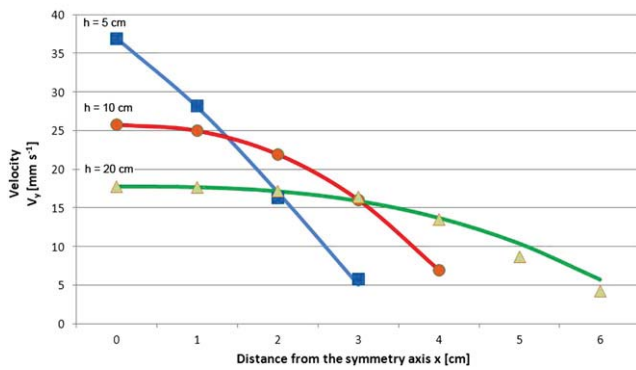


Fig. 8 – Variation of kinematic parameter  $B$  defined by Medina et al. (1998).



**Fig. 9 – Experimental measurements of vertical velocities at various levels and empirical values predicted by the parabolic model.**

(8) and (9) and the formula given in Medina et al. (1998), the kinematic parameter  $B$  depends on  $\hat{y}$  as:

$$B = 0.007e^2 \tag{6b}$$

Comparing the solutions given by other researchers, it can be stated that the prediction of the kinematic model qualitatively agrees with the conducted experiments. In each case a single fitting parameter  $b$  satisfactorily predicts the entire flow field. This fact indicates the most useful aspect of the kinematic model.

**5.2. Empirical description of vertical velocity  $V_y$  by a parabolic function**

An empirical description of vertical velocity  $V_y$  was proposed by the function:

$$V_y = V_0 \left[ 1 - A \left( \frac{x}{c} \right)^{\alpha} \right] \tag{7}$$

where:  $V_0$  is the initial velocity,  $x$  is the distance from the axis of symmetry,  $c$  is half of the width of the model, and  $A$  and  $\alpha$  – parameters, constant at the proper levels, determined by the LSM and presented in Table 4.

Readings taken at level $h$ (cm)	$A$	$\alpha$	$V_0$ (mm s <sup>-1</sup> )
5	4.745	1.162	36.92
10	10.913	2.295	25.75
20 and higher	5.373	2.678	17.77

According to the values given in Table A4, parameters  $A$ ,  $\alpha$ , and  $V_0$  (given in Eq. (7)) were assigned to the position of the levels, where the velocities were calculated. These parameters were determined according to the relationships:

$$\begin{aligned} A &= A_0 + A_1z + A_2z^2 \\ \alpha &= \alpha_0 + \alpha_1z + \alpha_2z^2 \\ V_0 &= V_{0_0} + V_{0_1}z + V_{0_2}z^2 \end{aligned} \tag{8}$$

A parabola was drawn across three points of the given coordinates  $((z_0, f(z_0)), (z_1, f(z_1)), (z_2, f(z_2)))$  using the Lagrange formula:

$$\begin{aligned} f(z) &= \frac{(z - z_1)(z - z_2)}{(z_0 - z_1)(z_0 - z_2)}f(z_0) + \frac{(z - z_0)(z - z_2)}{(z_1 - z_0)(z_1 - z_2)}f(z_1) \\ &+ \frac{(z - z_0)(z - z_1)}{(z_2 - z_0)(z_2 - z_1)}f(z_2) \end{aligned} \tag{9}$$

The parameters in Eq. (9);  $A$ ,  $\alpha$ , and  $V_0$  were calculated and  $f(z_i)$  are the values of parameters  $A$ ,  $\alpha$ , and  $V_0$ , for  $i = 0, 1, 2$  for levels  $h = 5, 10, 20$  cm in the model. The values of these parameters, presented in Table A4, are valid only for the range between heights  $h = 5$  cm and  $h = 20$  cm. For  $z$  from interval  $z \in (20, 50)$  the constant values of parameters  $A$ ,  $\alpha$ , and  $V_0$ , were calculated as for  $h = 20$  cm.

Using Eqs. (7) and (8), and the data given in Table 5, the empirical values of vertical velocity were determined and presented in Tables A10–A12 (in Electronic Appendix) where the average experimental values are also given for comparison. The goodness of fit between experimental and empirical values in the parabolic description of velocities is presented in Fig. 9.

For the remaining velocity profiles (i.e.  $h > 20$  cm), the agreement between the experimental measurements with the empirical model was good up to 4 cm from the axis of symmetry. At measurement points 5 and 6 cm from the axis of symmetry, the predicted values of vertical velocity by the empirical model did not agree as well as at the points closer to the symmetry axis (Table A12). At the higher levels, i.e.  $h > 20$  cm the velocities were uniform and the empirical description could be the same as used at all higher levels.

Parameter	$i = 0$	$i = 1$	$i = 2$
$A_i$	-7.382	3.021	-0.1192
$\alpha_i$	-0.5987	0.4149	-0.01255
$V_{0_i}$	52.88	-3.67	0.09573

**5.3. Verification of the accuracy of calculated velocities**

In Table 6 the comparison of the sums of the squares of differences of empirical and experimental values of velocities is given. Based on Figs. 4–6 it can be seen that comparing two empirical kinematic models a better description of velocity was obtained by using the modified model. But from the values given in Table A6 the best description was given by the parabolic function. The results from the modified empirical kinematic model and the parabolic model are very similar but the method of determining the parameters plays a significant role in the accuracy of the solution. In Table A6 it can be seen that using the modified empirical kinematic model the sum of the squares of the differences of velocities is 4–6 times less than the model given by Choi et al. (2005) and with the parabolic model the differences were even smaller (Tables 7–9).

**Table 6 – Comparison of the sums of the squares of the differences of velocities.**

Model	$\sum (V_{yempir} - V_{av})^2$ (R – correlation coefficient)		
	h (cm)		
	5	10	20 and higher
Gaussian	25.99 (0.9420)	50.23 (0.8479)	59.35 (0.9665)
Modified Gaussian	3.82 (0.9917)	12.95 (0.9631)	13.73 (0.9924)
Parabolic	1.22 (0.9974)	1.23 (0.9966)	5.29 (0.9971)

#### 5.4. Empirical description of the flow rate

##### 5.4.1. Empirical description of the flow rate using the kinematic and modified empirical functions

Flow rate is an important parameter in silos. An empirical analysis of the flow rate  $Q$  was developed based on descriptions given by the kinematic model of Choi et al. (2005) and the modified empirical kinematic model. For the area limited by the function described in Eq. (2), the limits of integration used in the calculations were:  $x_{max} = 4, 5, 7$  cm for the heights  $h = 5, 10, 20$  cm. The flow rate for the unit thickness was calculated numerically according to equation

$$Q = 2 \int_0^{x_{max}} Ae^{Bx^2} dx \quad (10)$$

at each level in the model and its values are given in Table A7.

**Table 7 – Comparison of flow rates calculated by applying the limits of integration  $x_{max} = 4, 5, 7$  cm.**

h (cm)		5	10	20 and higher levels
Q [ $10^{-1}$ cm <sup>2</sup> s <sup>-1</sup> ]	Gaussian	143.8	168.01	174.85
	Modified Gaussian	140.74	167.48	178.76
	model			

##### 5.4.2. Empirical description of the flow rate estimated by the parabolic function

On the basis of Eq. (7) the values of  $x_{max}$  were also determined but only for velocities  $V_y \geq 0$  using the relationship:

$$x_{max} = ce^{\frac{\ln A}{\alpha}} \quad x_{min} = 0 \quad (11)$$

where  $c = 13$  cm constitutes half of the width of the model and parameters  $A$  and  $\alpha$  are taken from Eq. (8) using the values listed in Table 5. The values  $x_{max}$  in Eq. (11) are given in Table 8 and denote the points where the parabola crosses the  $x$  axis.

The flow rate  $Q$  per unit thickness at a given level was calculated from Eq. (12) using Eq. (7) as an area limited by the following function

$$Q = 2 \int_0^{x_{max}} V_y dx = 2V_0 \left[ x_{max} - \frac{A}{c^\alpha (\alpha + 1)} x_{max}^{\alpha+1} \right] \quad (12)$$

**Table 8 – Values of the maximal distances from the symmetry axis  $x_{max}$ .**

Level h (cm)	5	10	20 and higher levels
Distance $x_{max}$ (cm)	3.397	4.587	6.939

Table 9 shows values of the flow rate but they are not constant and the laws of mass and volume conservation are not satisfied. This shows that the assumption of the constant density of the flowing material given by Drescher (1991) cannot be applied since the density of the material changes throughout the model. Density could be assumed to be approximately uniform and constant above level  $h = 20$  cm and higher where the velocities and the width of the funnel flow have similar values. However, the lowest flow rate was produced near to the outlet because the cross sectional area of funnel flow was at a minimum and velocity was at a maximum. The greater the height in the silo, the greater was the calculated values of the flow rate.

## 6. Empirical determination of the flow channel boundary (FCB)

In symmetrical flows the flow channel boundary was defined by Zhang and Ooi (1998) as the zone in which the particles do not slough off the solids surface but follow the paths predicted by the kinematic theory all the way to the outlet. The particles located in the surrounding feeding zone enter the top flow layer and roll down to the central axis; finally moving towards the outlet. Many investigations measuring and predicting the pattern of material flows during silo discharge have been carried out (e.g. Cundall & Strack, 1979; Nedderman & Tüzün, 1979). Tüzün and Nedderman (1979) defined the flow channel boundary as the streamline within which 99% of the total flow takes place whilst Watson and Rotter (1996) proposed to define the boundary where the velocity at each level is 1% of the centre line velocity at that level. Hence the vertical velocity was assumed  $V_y = 1\%$  at the stagnant zone boundary.

Using the readings from Tables A1–A6, given in the Electronic Appendix, the distances  $x_i$  (for instance  $x = 1, 2, 3, 4, 5$  cm) were determined from the axis of symmetry of the model. The values of  $x$  and the parameters of the proposed functions are given in Table A13 in Electronic Appendix. The last four readings of velocities  $V_y$  of non-zero values were taken for the analysis. If the 1% values of velocities in the assumed approximation were not obtained, as stated by Zhang and Ooi (1998), then another function was used to estimate the values. This occurred in only one such case.

On the basis of these data, the points of the calculated values of  $x$  at which vertical velocity  $V_y = 1\%$  are shown in

**Table 9 – Values of the flow rate  $Q$ .**

Level h (cm)	5	10	20 cm and higher levels
Flow rate Q [ $10^{-1}$ cm <sup>2</sup> s <sup>-1</sup> ]	135.1	164.6	179.55

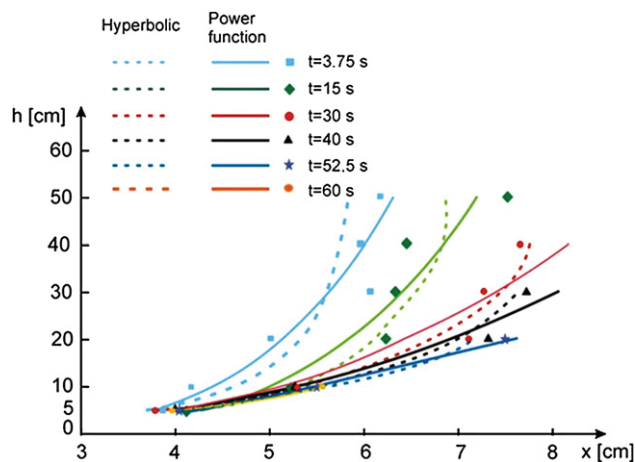


Fig. 10 – Range of the stagnant zone boundary at the analysed instants during flow.

Fig. 10. Two types of function were investigated to describe the relationship; power function

$$\hat{x} = a_1 z^{b_1} \quad (13)$$

and the hyperbolic function

$$\hat{x} = \frac{z}{a_2 + b_2 z} \quad (14)$$

Values of the parameters of these functions and the coefficients of correlation are given in Table A14.

## 7. Conclusions

An empirical analysis of velocities measured by the DPIV technique has been carried out. Velocity profiles obtained from the experiments were compared with empirical values. It was possible to approximate vertical velocity profiles inside the silo by means of a suitable regression function. Velocity was ascribed to the distance from the axis of symmetry and to the height in the model using an empirical description. For levels located higher than 20 cm above the outlet, vertical velocities reached stable values.

The theoretical analysis of velocities in the model was presented in two parts: by applying the Gaussian function based on the model presented by Choi et al. (2005) and by using a modified empirical kinematic model. The modified model described velocity more accurately than the Gaussian model. This was confirmed by the statistical analysis presented. The sum of the squares of differences of the empirical and experimental values of velocities for the modified model was several times lower than for the model presented by Choi et al. (2005). However, the best description of velocity was given by a parabolic function. This was followed by the modified empirical kinematic function and then the Gaussian function of Choi et al. (2005). There were no significant differences between the two models used to describe the flow rates.

It was found that kinematic parameter  $b$  defined by Choi et al. (2005) depended on the height in the model and varied considerably in the vicinity of the outlet. In this region its

increase was the highest. Above 10 cm from the outlet the increase in  $b$  was imperceptible and its value stabilised to the values that were different from those given in Medina et al., 1998.

## Acknowledgements

The authors wish to thank to Prof. Zenon Mróz of Institute of Fundamental Technological Research of Polish Academy of Sciences in Warsaw, Poland for all suggestions concerning the empirical description of the problem presented in this paper. The paper was partly prepared under the project S/WM/2/08. Special thanks are directed to Slawomir Blonski, PhD for the images made in the DPIV technique.

## Appendix. Supplementary materials

Supplementary data related to this article (Electronic Appendix) can be found online at doi:10.1016/j.biosystemseng.2011.01.004.

## REFERENCES

- Beverloo, W. A., Leniger, H. A., & de Velde, J. V. (1961). The flow of granular solids through orifices. *Chemical Engineering Science*, 15, 260–268.
- Böhmsen, J. U., Ostendorf, M., Antes, H., & Schwedes, J. (2004). Silo discharge: measurement and simulation of dynamic behaviour in bulk solids. *Chemical Engineering Technology*, 27, 71–76.
- Brown, R. L., & Richards, J. C. (1970). *Principles of powder mechanics*. New York: Pergamon.
- Choi, J., Kudrolli, A., & Bazant, M. Z. (2005). Velocity profile of granular flows inside silos and hoppers. *Journal of Physics Condensed Matter*, 17, S2533–S2548.
- Cundall, P. A., & Strack, O. D. L. (1979). A discrete numerical model for granular assemblies. *Geotechnique*, 29, 47–65.
- Drescher, A. (1991). *Analytical methods in bin-load analysis*. Amsterdam: Elsevier.
- Drescher, A., & Ferjani, M. (2004). Revised model for plug/funnel flow in bins. *Powder Technology*, 141, 44–54.
- Häussler, U., & Eibl, J. (1984). Numerical investigations on discharging silos. *Journal of Engineering Mechanics Division, ASCE*, 110(EM6), 957–971.
- Hirshfeld, D., Radzyner, Y., & Rapaport, D. C. (1997). Molecular dynamics studies of granular flow through an aperture. *Physics Review E*, 56(4), 4404–4415.
- Hong, D. C., & McLennan, J. A. (1992). Molecular dynamics simulations of hard sphere granular particles. *Physica A*, 187(1–2), 159–171.
- Jenike, A. W. (1961). *Gravity flow of bulk solids*. USA: University of Utah Engineering Experiment Station, Bulletin 108.
- Jenike, A. W. (1964). *Storage and flow of solids*. USA: University of Utah Engineering Experiment Station, Bulletin 123.
- Kafui, K. D., & Thornton, C. (1997). In Behringer, & Jenkins. (Eds.), *Some observations on granular flow in hoppers and silos, powders & grains'97* (pp. 511–514). Balkema.
- Khelil, A., & Roth, J. C. (1994). Gravitational flow behaviour of granular materials. *European Journal of Mechanics B/Fluids*, 13(1), 57–72.

- Litwiniszyn, J. (1963). The model of a random walk of particles adopted to researches on problem of mechanics of loose media. *Bulletin L'Academie Polonaise Sciences*, 11, 61–70.
- Lueptow, R. M., Akonur, A., & Shinbrot, T. (2000). PIV for granular flows. *Experiments in Fluids*, 28(2), 183–186.
- Medina, A., Córdova, J. A., Luna, E., & Treviño, C. (1998). Velocity field measurements in granular gravity. *Physics Letters A*, 250, 111–116.
- Mullins, W. W. (1972). Stochastic theory of particle flow under gravity. *Journal of Applied Physics*, 43, 665–677.
- Mullins, W. W. (1974). Experimental evidence for the stochastic theory of particle flow under gravity. *Powder Technology*, 9, 29–37.
- Mullins, W. W. (1979). Critique and comparison of two stochastic theories of gravity-induced particle flow. *Powder Technology*, 23, 115–119.
- Nedderman, R. M. (1992). *Statics and kinematics of granular materials*. New York: Cambridge University Press.
- Nedderman, R. M. (1995). The use of the kinematic model to predict the development of the stagnant zone boundary in the batch discharge of a bunker. *Chemical Engineering Science*, 50, 959–965.
- Nedderman, R. M., & Tüzün, U. (1979). A kinematic model for the flow of granular materials. *Powder Technology*, 22, 243–253.
- Niedostatkiewicz, M., & Tejchman, J. (2005). Application of a particle image velocimetry technique for deformation measurements of bulk solids during silo flow. *Powder Handling & Processing*, 17(4), 216–220.
- Ooi, J. Y., Chen, J. F., & Rotter, J. M. (1998). Measurement of solids flow patterns in a gypsum silo. *Powder Technology*, 99, 272–284.
- Ostendorf, M., & Schwedes, J. (2005). Application of particle image velocimetry for velocity measurements during silo discharge. *Powder Technology*, 158, 69–75.
- Quenot, G. M., Pakleza, J., & Kowalewski, T. A. (1998). Particle image velocimetry with optical flow. *Experiments in Fluids*, 25, 177–189.
- Sakaguchi, H., Ozaki, E., & Igarashi, T. (1993). Plugging of the flow of granular materials during the discharge from a silo. *International Journal of Modern Physics B (IJMPB)*, 7(9/10), 1949–1963.
- Samadani, A., Pradhan, A., & Kudrolli, A. (1999). Size segregation of granular matter in silo discharges. *Phys. Rev. E*, 60, 7203.
- Sielamowicz, I., Błoński, S., & Kowalewski, T. A. (2005). Optical technique DPIV in measurements of granular material flows, part 1 of 3-plane hoppers. *Chemical Engineering Science*, 60(2), 589–598.
- Sielamowicz, I., Błoński, S., & Kowalewski, T. A. (2006). Digital particle image velocimetry (DPIV) in measurements of granular material flows, part 2 of 3-converging hoppers. *Chemical Engineering Science*, 6(2), 5307–5317.
- Sielamowicz, I., Czech, M., & Kowalewski, T. A. (2010). Empirical description of flow parameters in eccentric flow inside a silo model. *Powder Technology*, 198, 381–394.
- Srinivasa, M. L., Nott, P. R., & Kesava, R. K. (1997). Fully developed flow of coarse granular materials through a vertical channel. *Chemical Engineering Science*, 52(6), 913–933.
- Steingart, D. A., & Evans, J. W. (2005). Measurements of granular flows in two dimensional hoppers by particle image velocimetry. Part I: experimental method and results. *Chemical Engineering Science*, 60, 1043–1051.
- Tüzün, U., Houlsby, G. T., Nedderman, R. M., & Savage, S. B. (1982). The flow of granular materials – II: velocity distributions in slow flow. *Chemical Engineering Science*, 37, 1691–1709.
- Tüzün, U., & Nedderman, R. M. (1979). Experimental evidence supporting kinematic modelling of the flow of granular media in the absence of air drag. *Powder Technology*, 24, 257–266.
- Wang, F., Gardner, C., & Schaeffer, D. G. (1992). Steady-state computation of granular or in an axisymmetric hopper. *SIAM Journal of Applied Mathematics*, 52, 1076.
- Waters, A. J., & Drescher, A. (2000). Modelling plug flow in bins/hoppers. *Powder Technology*, 113, 168–175.
- Watson, G. R., & Rotter, J. M. (1996). A finite element analysis of planar granular solids flow. *Chemical Engineering Science*, 51(16), 3967–3978.
- Zhang, K. F., & Ooi, J. Y. (1998). A kinematic model for solids flow in flat-bottomed silos. *Geotechnique*, 48(4), 545–553.